

# Synchronization experiments with an atmospheric global circulation model

Frank Lunkeit<sup>a)</sup>

*Meteorologisches Institut, Universität Hamburg, Bundesstrasse 55, D-20146 Hamburg, Germany*

(Received 14 August 2000; accepted for publication 9 November 2000)

Synchronization in a chaotic system with many degrees of freedom is investigated by coupling two identical global atmospheric circulation models. Starting from different initial conditions, the two submodels show complete synchronization as well as noncomplete synchronization depending on the coupling strength. The relatively low value of the coupling strength threshold for complete synchronization indicates the potential importance of synchronization mechanisms involved in climate variability. In addition, the results suggest synchronization experiments as a valuable additional method to analyze complex dynamical models, e.g., to estimate the largest Lyapunov exponent. © 2001 American Institute of Physics. [DOI: 10.1063/1.1338127]

**Components of the climate system like the atmosphere and oceans exhibit some coherent variability. Synchronization might be one process relating fluctuations of different subsystems even if the coupling is weak. Synchronization of chaos is a well-known phenomenon and extensively studied. For the high dimensional climate system, however, the degree of synchronization in relation to the strength of the coupling is not *a priori* clear. We address this question by coupling to identical atmospheric circulation models. In this ideal case complete synchronization is obtained by relatively weak coupling. In addition, we demonstrate that synchronization experiments may be used to estimate the largest Lyapunov exponent of complex models.**

extent synchronization can be expected in real geophysical fluids like, for example, the coupled atmosphere ocean system. In this paper we address this question by coupling two identical atmospheric global circulation models. This configuration has the advantage to allow, in principle, complete synchronization (if the coupling strength goes to infinity) and no synchronization (if the coupling strength goes to zero). The motivation is to investigate the properties of synchronization in the presumably most ideal case before considering the complicated interaction between the climate subsystems of quite different behavior. Section II describes the model and the experimental setup. Synchronization of the two models depending on the strength of a bidirectional coupling for all prognostic variables is investigated in Sec. III. Section IV summarizes and discusses the results.

## I. INTRODUCTION

Synchronization of coupled nonlinear systems exhibiting chaotic behavior is well documented for low order systems. It is found that coupled identical systems obtain complete synchronization under certain conditions. Nonidentical systems may show phase synchronization [Rosenblum *et al.* (1996)], lag synchronization [Rosenblum *et al.* (1997)], or generalized synchronization [Rulkov *et al.* (1995)]. Bidirectional coupling [Fujisaka and Yamada (1983)] and drive/response setups [Pecora and Carroll (1990)] are familiar configurations to study synchronization. Also for complex coupled systems, different degrees of synchronization are documented [e.g., Osipov *et al.* (1997); Bünner and Just (1998); Boccaletti *et al.* (1999a); Boccaletti *et al.* (1999b); Boccaletti *et al.* (2000)].

With respect to the climate system, synchronization of coupled subsystems (such as atmosphere–ocean or stratosphere–troposphere) may be an important process contributing to the observed variability. Duane (1997), for example, finds partial synchronization between the two hemispheres in a low order atmospheric model and presents some observational evidence. However, it is still not clear to what

## II. MODEL AND SIMULATIONS

### A. Model

We utilize the Portable University Model of the Atmosphere (PUMA) [Fraedrich *et al.* (1998)], which has demonstrated to be an appropriate tool to analyze various aspects of the atmospheric dynamics [Frisius *et al.* (1998); von Hardenberg *et al.* (2000)]. PUMA represents the dynamical core of a state-of-the-art spectral atmospheric general circulation model (AGCM) being used in present day weather forecast and climate simulations [Holten (1992)]. The dry primitive equations for the atmospheric fluid on a sphere are integrated using the spectral transform method [Orszag (1970)]: Linear terms are evaluated in the spectral domain while nonlinear products are calculated in grid point space. Temperature, divergence, vorticity, and the logarithm of the surface pressure are the prognostic variables. The vertical is divided into equally spaced  $\sigma$  levels ( $\sigma = p/p_s$ , where  $p$  and  $p_s$  denote the pressure and the surface pressure, respectively). The integration in time is carried out with a filtered leap-frog semi-implicit scheme [Robert (1966)]. For our experiments we chose five vertical levels and a T21 horizontal resolution (i.e., the series of spectral harmonics representing the prognostic variables are triangular truncated at total wave number

<sup>a)</sup>Electronic mail: lunkeit@dkrz.de

21, which is approximately  $5.6^\circ \times 5.6^\circ$  on the corresponding Gaussian grid). This leads to a total number of 8096 dynamical variables.

While the representation of the atmospheric dynamic is similar to a full state-of-the-art AGCM, the representation of diabatic and subscale processes in PUMA is very simple and linear: A hyperdiffusion ( $\propto \nabla^8$ ) applied to temperature, divergence, and vorticity represents the effect of subgrid scale eddies. Rayleigh friction acting on divergence and vorticity provides the large scale dissipation (i.e., a term  $-x/\tau_f$  is added to the equations for divergence and vorticity, where  $\tau_f$  is the friction time scale and  $x$  is the respective variable). The model is driven by a Newtonian cooling formulation for the diabatic heating: The model temperature is relaxed toward a prescribed reference temperature [i.e., a term  $+(T_R - T)/\tau_c$  is added to the temperature equations, where  $\tau_c$  is the heating/cooling time scale,  $T$  denotes the actual model temperature, and  $T_R$  refers to the prescribed reference temperature].

The complete equations of the PUMA model are written as

$$\frac{\partial \zeta}{\partial t} = \frac{1}{1 - \mu^2} \frac{\partial}{\partial \lambda} \mathcal{F}_v - \frac{\partial}{\partial \mu} \mathcal{F}_u - \frac{\zeta}{\tau_f} - K \nabla^8 \zeta, \quad (1)$$

$$\begin{aligned} \frac{\partial D}{\partial t} = & \frac{1}{1 - \mu^2} \frac{\partial}{\partial \lambda} \mathcal{F}_u + \frac{\partial}{\partial \mu} \mathcal{F}_v \\ & - \nabla^2 \left( \frac{U^2 + V^2}{2(1 - \mu^2)} + \Phi + \bar{T} \ln p_s \right) - \frac{D}{\tau_f} - K \nabla^8 D, \end{aligned} \quad (2)$$

$$\begin{aligned} \frac{\partial T'}{\partial t} = & - \frac{1}{1 - \mu^2} \frac{\partial}{\partial \lambda} (UT') - \frac{\partial}{\partial \mu} (VT') + DT' \\ & - \dot{\sigma} \frac{\partial T}{\partial \sigma} + \kappa \frac{T\omega}{p} + \frac{T_R - T}{\tau_c} - K \nabla^8 T', \end{aligned} \quad (3)$$

$$\frac{\partial \ln p_s}{\partial t} = - \frac{U}{1 - \mu^2} \frac{\partial}{\partial \lambda} \ln p_s - V \frac{\partial}{\partial \mu} \ln p_s - D - \frac{\dot{\sigma}}{\partial \sigma}, \quad (4)$$

$$\frac{\partial \Phi}{\partial \ln \sigma} = -T, \quad (5)$$

where  $\zeta$  and  $\xi$  denote absolute and relative vorticity, respectively.  $D$  is the horizontal divergence and  $p_s$  the surface pressure. The temperature  $T$  is divided into a background state,  $\bar{T}$ , and an anomaly,  $T'$ . In addition,  $\lambda$  and  $\phi$  are longitude and latitude respectively,  $\mu = \sin \phi$ ,  $\Phi$  is the geopotential,  $\kappa$  is the adiabatic coefficient,  $\omega$  is vertical velocity, and  $K$  a diffusion coefficient. We also use the abbreviations  $U = u \cos \phi$  and  $V = v \cos \phi$  ( $u, v$  are the zonal and meridional velocities, respectively),  $\mathcal{F}_u = V\zeta - \dot{\sigma}(\partial U/\partial \sigma) - T'(\partial \ln p_s/\partial \lambda)$  and  $\mathcal{F}_v = -U\zeta - \dot{\sigma}(\partial V/\partial \sigma) - T'(1 - \mu^2) \times (\partial \ln p_s/\partial \mu)$ .

Equations (1) and (2) are the vorticity and divergence equations, respectively. Equation (3) is the thermodynamic

equation, Eq. (4) is the conservation of mass (continuity), and Eq. (5) expresses hydrostatic equilibrium in  $\sigma$  coordinates.

All simulations described in the following use the same boundary conditions, which are defined by the following characteristics of the model setup: The distribution of the relaxation temperature for the Newtonian cooling,  $T_R$ , is zonally symmetric with an equator pole difference of 80 K for both hemispheres (equinox conditions). A lapse rate of 0.0065 K/m defines the vertical temperature profile in the troposphere. The Newtonian cooling relaxation time scale,  $\tau_c$ , is 30 days for all levels. Rayleigh friction is confined to the lowermost level with a time scale  $\tau_f$  of one day. The hyperdiffusion acts on all waves and damps the smallest resolved wave with a time scale of 0.25 days. A time step of 1 h is used. No external variability like annual or daily cycle is imposed.

## B. Coupling

Two identical PUMA models ( $M_1$  and  $M_2$ ) are symmetrically coupled. The coupling formulation follows the bulk aerodynamic parametrization for fluxes between subsystems as being used in climate models (e.g., for the ocean-atmosphere heat flux). In our experiments, however, we couple all prognostic variables and do not restrict the coupling to a subset of them. For systematic analysis a linear coupling is chosen, i.e., the transfer coefficient is represented by a constant ‘‘coupling strength’’ independent of the states of the submodels. The equations of the coupled model may be written as

$$\begin{aligned} \dot{X}_1 = & \text{PUMA}(X_1) + \frac{1}{\epsilon}(X_2 - X_1), \\ \dot{X}_2 = & \text{PUMA}(X_2) + \frac{1}{\epsilon}(X_1 - X_2), \end{aligned} \quad (6)$$

where  $X_1$  and  $X_2$  are the state vectors of  $M_1$  and  $M_2$ , respectively, combining temperature, divergence, vorticity, and the logarithm of the surface pressure.  $\text{PUMA}(X_{1,2})$  denotes the nonlinear model operator [i.e., Eqs. (1)–(5)]. The time scale of the coupling (or the coupling strength),  $\epsilon$ , is chosen to be the same for all variables. This time scale may later on be compared with the external time scales  $\tau_c$  and  $\tau_f$  for the Newtonian cooling and the Rayleigh friction.

## C. Simulations

A set of simulations using the boundary conditions described in Sec. II A is performed with different values of the coupling time scale  $\epsilon$  ranging from 5 days to 30 days (actually, we performed integrations for  $\epsilon = 5, 6, 7, 8, 9, 10, 12.5, 15, 17.5, 20, 22.5, 25, 25.5, 26, 28, \text{ and } 30$  days). A run without coupling serves as a reference integration.

All simulations are at least 36 000 days long and start from the same initial conditions for the submodels, which are obtained by the following initialization procedure: Both atmospheres are integrated from a resting state, that is no winds and no horizontal temperature gradients, plus a small surface pressure perturbation, which is different for  $M_1$  and

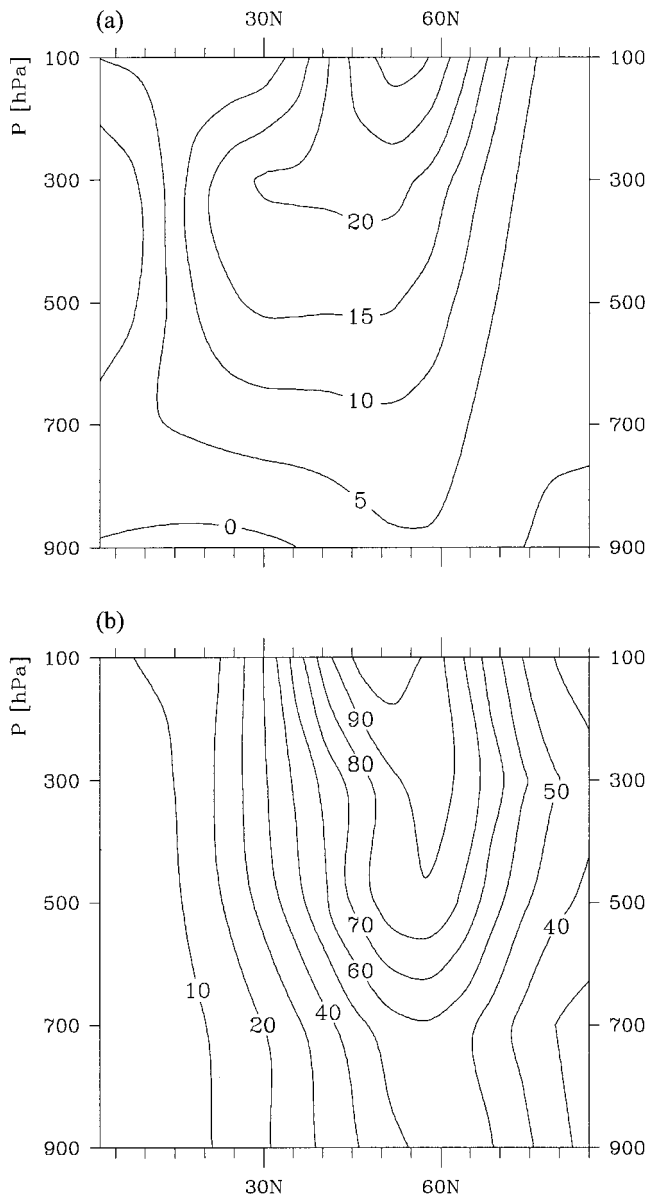


FIG. 1. Northern hemisphere cross sections of the zonal and time mean zonal wind (m/s) (a), and the geopotential height standard deviation (m) (b).

$M_2$ . The models run 360 days without coupling including a spin up of about 90 days after which a quasistationary state with fully evolved internal variability is reached. The final states of both models serve as the initial conditions for the coupled simulations. Due to the different initial conditions at the beginning of the spin up, the deviations of  $M_1$  and  $M_2$  from the mean climate are independent. The results concerning the synchronization, however, do not qualitatively depend on the specific choice of the model parameters or the initial conditions.

The model climate obtained by the chosen parameter setting (similar for all simulations) is illustrated in Fig. 1, which shows northern hemisphere cross sections of the zonal and time mean zonal wind (a) and the geopotential height standard deviation (b). Despite all simplifications concerning the parametrizations, the model simulates major features of the observed zonally averaged atmospheric circulation. Both

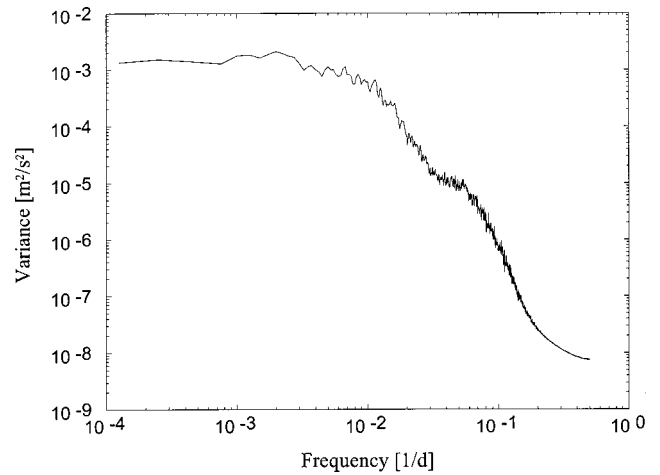


FIG. 2. Power spectrum of the  $\bar{\xi}_1^0$  anomalies for one submodel during the reference run.

the tropical easterlies and the westerly jets are captured by the model. Also, the eddy activity in the midlatitudes is reproduced. The time behavior of the submodels is diagnosed using the gravest zonal wave number 0 spectral component of the relative vorticity, averaged with respect to  $\sigma$ . This variable,  $\bar{\xi}_1^0$ , represents the global mean relative angular velocity and is, in general, positive (indicating the superrotation of the atmosphere). Figure 2 gives the power spectrum,  $|\hat{\xi}(\omega)|^2$ , of the  $\bar{\xi}_1^0$  anomalies ( $\hat{\xi}(\omega) = \int \bar{\xi}_1^0(t) e^{i\omega t} dt$ ) for one submodel calculated from the 36 000 days of the reference run (daily data excluding the initial 360 days). The submodel exhibits variability on all time scales. The overall slope of the spectrum is somewhat steeper than  $\omega^{-2}$  with enhanced variability on time scales of the model’s synoptic activity (approximately 5–50 days). This spectrum is representative for a broad range of parameter configurations.

### III. SYNCHRONIZATION

The transition to synchronization of the two subsystems during the coupled integrations may be estimated using the differences between  $\bar{\xi}_1^0$  of the two subsystems ( $\Delta \bar{\xi}_1^0 = |\bar{\xi}_1^0(M_1) - \bar{\xi}_1^0(M_2)|$ ). This measure, however, is of global scale (wave number one) and represents a small number (five) of the prognostic variables for each submodel only. Therefore, we also calculate the root mean squared difference of the 500 hPa geopotential height field between the models,  $\text{rms}(z_{500})$ . This parameter (a typical meteorological measure for, e.g., the quality of a forecast) combines a large number of degrees of freedom and represents all space scales resolved by the model (up to wave number 21). In particular, it puts more emphasis on disturbances like synoptic eddies. Figure 3 shows the time evolution of  $\text{rms}(z_{500})$  for the integration with coupling time scale  $\epsilon = 10, 20,$  and 30 days. In the  $\epsilon = 10$  day run, the  $\text{rms}(z_{500})$  decays quite rapidly to zero. Complete synchronization is reached after about 150 days. We use the term ‘‘complete synchronization’’ if both the  $\text{rms}(z_{500})$  and the  $\Delta \bar{\xi}_1^0$  are zero (in the limit of the numerical precision of the model output, which is a 16 bit

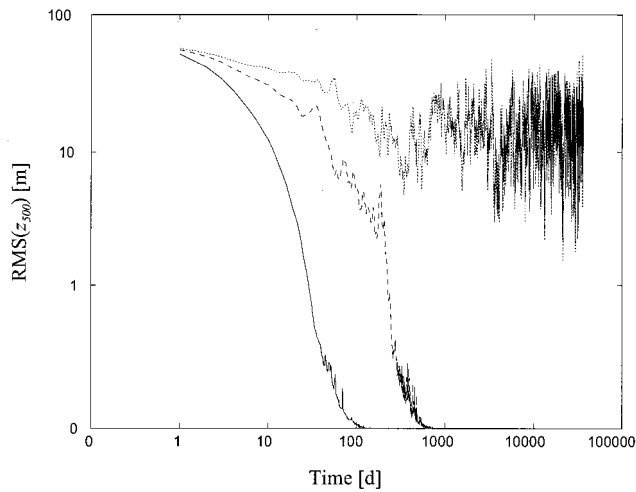


FIG. 3. Time evolution of rms ( $z_{500}$ ) for the integration with coupling time scale  $\epsilon=10$  days (solid curve), 20 days (dashed curve), and 30 days (dotted curve) (axis in logarithmic scaling).

reduction of the original 64 bit model variables) for the rest of the simulation, which is at least as long as the transition phase.

Decreasing the coupling strength (increasing  $\epsilon$  from 10 to 20 days) leads to an increase of the decay time. In the beginning, all simulations show an exponential decay with a time scale of about  $\epsilon/2$ . However, while complete synchronization is also obtained in the  $\epsilon=20$  day run, the state of both submodels remains different after 36 000 days in the  $\epsilon=30$  day simulation. In this run, the rms ( $z_{500}$ ) saturates after the decay, with an average of approximately 18 m, which is about 25% of the averaged rms ( $z_{500}$ ) in the reference integration. The time scale on which the variability of the two submodels is related may be analyzed by the squared coherence spectrum,  $|\hat{S}(\omega)|^2 = A^2(\omega) |\hat{\xi}_1(\omega)|^2 |\hat{\xi}_2(\omega)|^2$ , for the  $\bar{\xi}_1^0$  anomalies. Here,  $A$  results from decomposing the complex cross spectrum,  $C(\omega) = \hat{\xi}_1(\omega) \hat{\xi}_2^*(\omega)$ , into amplitude and phase,  $C = A \exp(i\phi)$ . The  $|\hat{S}(\omega)|^2$  spectrum [Fig. 4(a)] computed for the last 30 000 days of the integration indicates that the difference is mostly confined to variability on synoptic time scales (5–50 days). For these time scales, the squared coherence decreases to lower, but still significant, values of about 0.85. However, it should be pointed out that the results from the coherence spectrum are only a first indication for an interrelation of the subcomponents. Tass *et al.* (1998) show that coherence is often not an appropriate quantity to reveal hidden synchronization.

While the coupling leads to a synchronization, it appears not to affect the general feature of the time behavior of the submodels, as can be seen by comparing the power spectra of one submodel in the coupled run [Fig. 4(b)] and the submodel in the uncoupled reference simulation (Fig. 2).

A comprehensive picture of the synchronization characteristic of the model is given in Fig. 5, where the inverse of the time needed for complete synchronization,  $1/T_S$ , is plotted against the coupling strength  $1/\epsilon$ . We define  $T_S$  as the last time where we observed a rms ( $z_{500}$ ) greater than zero. The curve indicates a linear relation of those two quantities.

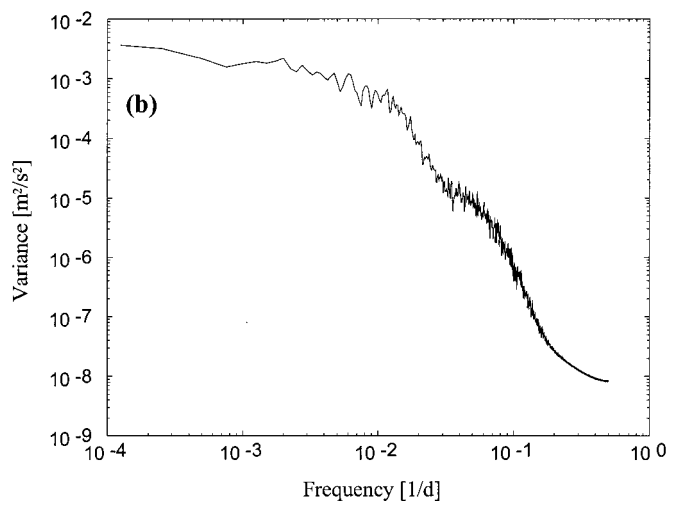
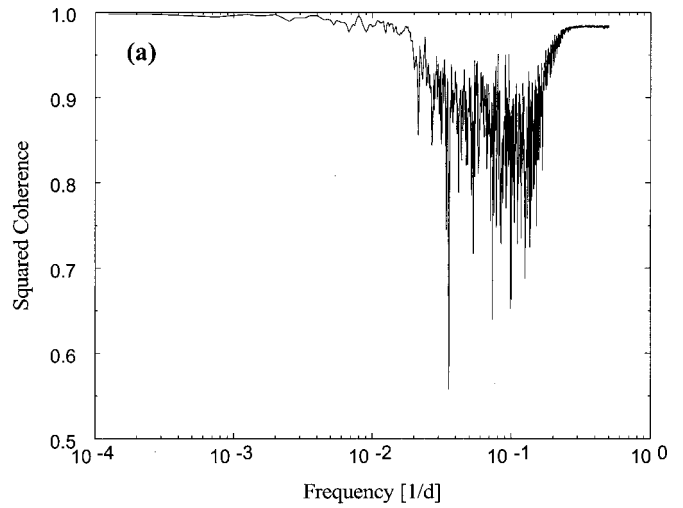


FIG. 4. (a) Squared coherence spectrum for the  $\bar{\xi}_1^0$  anomalies of the two submodels in the  $\epsilon=30$  day integration. (b) Power spectrum of the submodels in the  $\epsilon=30$  day integration. Both spectra calculated from the last 30 000 days.

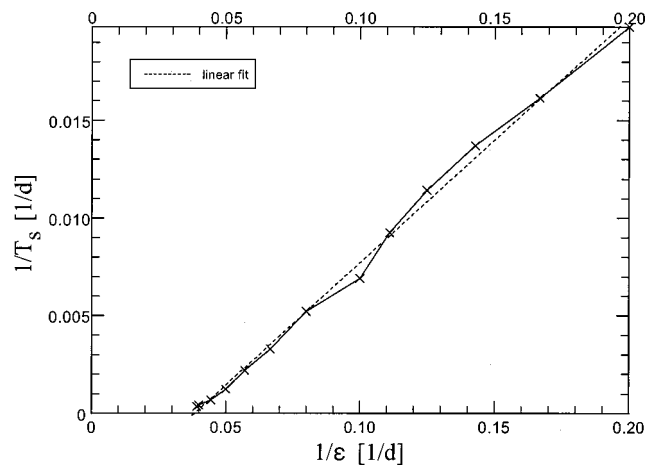


FIG. 5. Inverse of the time needed for complete synchronization,  $1/T_S$ , vs coupling strength  $1/\epsilon$  (solid curve, crosses indicate the actual experiments) and the corresponding linear fit (dashed line).

The intercept of the linear fit with the  $(1/\epsilon)$  axis at  $1/\epsilon=0$  suggests a coupling time scale threshold close to 26 days for complete synchronization. Indeed, the submodels do not synchronize completely in a 72 000 days integration with  $\epsilon=26$  days. In this run, the rms ( $z_{500}$ ) stays at very small values after the initial decay.

#### IV. DISCUSSION AND CONCLUSION

The investigation indicates that complete synchronization can be found in coupled chaotic systems with many degrees of freedom. Our symmetrically coupled atmospheric circulation models show complete synchronization with a fairly weak coupling, that is a coupling time scale up to values comparable to the tropospheric radiative equilibrium time scale. Complete synchronization is not obtained if the coupling time scale exceeds a threshold value of about 26 days. Sensitivity experiments (not discussed in this paper) show that there is no strong relation between the threshold and the time scale of the Newtonian cooling as might be expected from the approximate agreement of these values in our experiments.

If the submodels do not synchronize completely, the average distance in phase space, as measured by the rms ( $z_{500}$ ), is still smaller than in the uncoupled case. In addition, the difference is mostly confined to a distinct frequency band, related to the synoptic activity in the model. These results may indicate that only a subset of modes synchronize for a given coupling strength, while others do not. It is well known that low order systems exhibit complete synchronization if the coupling strength exceeds half the largest Lyapunov exponent and synchronization experiments are suggested to be used as a possible way to estimate this exponent [Fujisaka and Yamada (1983)]. For our model, the threshold value of  $\epsilon=26$  days would correspond to a Lyapunov exponent of about 0.08/day. However, this value is hard to validate. Estimates of the largest Lyapunov exponent from the model time series by applying the Wolf *et al.* algorithm [Wolf *et al.* (1985)] and the TISEAN package [Hegger *et al.* (1999)] do not give robust results. The numbers obtained from these analysis tools range from about 0.2 to 0.01/day and appear to be very sensitive to the embedding delay, the propagation time, etc. Therefore, the use of synchronization experiments may indeed be an attractive alternative, in particular if we consider the quite small uncertainties of the linear fit in Fig. 5.

In summarizing our results, two main conclusions may be drawn: (i) Synchronization can be one important mechanism involved in climate variability. However, since the climate subsystems are not identical as in our example, complete synchronization is not possible, but generalized or phase synchronization is likely. This will be the focus of future studies utilizing submodels with parameter mismatches of increasing magnitude. (ii) Synchronization experiments can improve the understanding of complex sys-

tems and may help to derive dynamical properties such as characteristic time scales (or Lyapunov exponents) and associated patterns.

#### ACKNOWLEDGMENTS

The author wishes to thank Jürgen Kurths for encouraging this work. Many useful comments from Klaus Fraedrich, Richard Blender, and Frank Sielmann are gratefully acknowledged. The work was supported by the BMBF under Grant No. 07KFT121.

- Boccaletti, S., Bragard, J., and Arecchi, F. T. (1999a). "Controlling and synchronizing space time chaos," *Phys. Rev. E* **59**, 6574–6578.
- Boccaletti, S., Bragard, J., Arecchi, F. T., and Mancini, H. (1999b). "Synchronization in nonidentical extended systems," *Phys. Rev. Lett.* **83**, 536–539.
- Boccaletti, S., Valladares, D. L., Kurths, J., Maza, D., and Mancini, H. (2000). "Synchronization of chaotic structurally nonequivalent systems," *Phys. Rev. E* **61**, 3712–3715.
- Bünner, M. J. and Just, W. (1998). "Synchronization of time-delay systems," *Phys. Rev. E* **58**, R4072–R4075.
- Duane, G. S. (1997). "Synchronized chaos in extended systems and meteorological teleconnections," *Phys. Rev. E* **56**, 6475–6493.
- Fraedrich, K., Kirk, E., and Lunkeit, F. (1998). "PUMA: Portable University Model of the Atmosphere," Deutsches Klimarechenzentrum Technical Report No. 16.
- Frisius, T., Lunkeit, F., Fraedrich, K., and James, I. N. (1998). "Storm-track organization and variability in a simplified global circulation model," *Q. J. R. Meteorol. Soc.* **124**, 1019–1043.
- Fujisaka, H. and Yamada, T. (1983). "Stability theory of synchronized motion in coupled-oscillator systems," *Prog. Theor. Phys.* **69**, 32–47.
- Hegger, R., Kantz, H., and Schreiber, T. (1999). "Practical implementation of nonlinear time series methods: The TISEAN package," *Chaos* **9**, 413–435.
- Holton, J. R. (1992). *An Introduction to Dynamic Meteorology*, 3rd ed. (Academic, New York).
- Orszag, S. A. (1970). "Transform method for calculation of vector coupled sums: Application to the spectral form of the vorticity equation," *J. Atmos. Sci.* **27**, 890–895.
- Osipov, G. V., Pikovsky, A. S., Rosenblum, M. G., and Kurths, J. (1997). "Phase synchronization effects in a lattice of nonidentical Rössler oscillators," *Phys. Rev. E* **55**, 2353–2361.
- Pecora, L. and Carroll, T. (1990). "Synchronization in chaotic systems," *Phys. Rev. Lett.* **64**, 821–824.
- Robert, A. (1966). "The integration of a low order spectral form of the primitive meteorological equations," *J. Meteorol. Soc. Jpn.* **44**, 237–245.
- Rosenblum, M. G., Pikovsky, A. S., and Kurths, J. (1996). "Phase synchronization of chaotic oscillators," *Phys. Rev. Lett.* **76**, 1804–1807.
- Rosenblum, M. G., Pikovsky, A. S., and Kurths, J. (1997). "From phase to lag synchronization in coupled chaotic oscillators," *Phys. Rev. Lett.* **78**, 4193–4196.
- Rulkov, N. F., Sushchik, M. M., Tsimring, L. S., and Abarbanel, H. D. I. (1995). "Generalized synchronization of chaos in directionally coupled chaotic systems," *Phys. Rev. E* **51**, 980–994.
- Tass, P., Rosenblum, M. G., Weule, J., Kurths, J., Pikovsky, A., Volkman, J., Schnitzler, A., and Freund, H.-J. (1998). "Detection of  $n:m$  phase locking from noisy data: Application to magnetoencephalography," *Phys. Rev. E* **81**, 3291–3294.
- von Hardenberg, J., Fraedrich, K., Lunkeit, F., and Provenzale, A. (2000). "Transient chaotic mixing during a baroclinic life cycle," *Chaos* **10**, 122–134.
- Wolf, A., Swift, J. B., Swinny, H. L., and Vastano, J. A. (1985). "Determining Lyapunov exponents from a time series," *Physica D* **16**, 285–317.